Alkali-metal-fulleride phase equilibria

D. M. Poirier, D. W. Owens, and J. H. Weaver
Department of Materials Science and Chemical Engineering, University of Minnesota, Minneapolis, Minnesota 55455
(Received 25 May 1994)

The binary phase diagrams of the alkali-metal fullerides, A_xC_{60}, are discussed in light of recent experimental results concerning the A_1C_{60} phases and their transformations. The Rb_1C_{60} and Cs_1C_{60} phases undergo diffusionless structural transformations upon cooling and their phase diagrams require solutions that differ from the eutectoid transformation of K_1C_{60}. X-ray photoelectron spectroscopy has been used to characterize these transformations. Phase diagrams incorporating two invariant reactions are proposed. The equilibrium vapor pressure of C_{60} has been determined at lower temperatures than prevously examined and the pure C_{60} phase diagram has been assembled for a large range of temperature and pressure. The predicted effects of solid-solution formation on the fcc to simple cubic transition of α-C_{60} are discussed in terms of eutectoid and peritectoid phase-diagram topologies. High-temperature decomposition with fractional sublimation has been used to gain insight into the relative thermal stabilities of the various compounds. Using this information and data from the literature, a K_xC_{60} phase diagram extending to vaporization temperatures is proposed.

I. INTRODUCTION

When Haddon *et al.*[1] first reported alkali-metal reaction with C_{60} films, the nature of the metal-fulleride material formed was not known. In particular, it was not clear whether a homogeneous solid solution of metal atoms formed within the fcc C_{60} matrix or if phase-separated compounds were produced. The discovery of superconductivity in K_xC_{60} provided great impetus to learn more about these systems.[2–4] Holzcer *et al.*[4] provided evidence that a distinct phase with the composition $x=3$ was responsible for the observed superconductivity in K_xC_{60}. Further, photoemission[5,6] and nuclear magnetic resonance[7] (NMR) experiments on K_xC_{60} indicated that samples with compositions between $x=0$ and 3 were composed of phase-separated K_3C_{60} and essentially pure C_{60}. Subsequent work has supported this picture of phase separation for noninteger global stoichiometries.[8–13]

The nearly spherical shape of C_{60} and the ionic bonding in the A_xC_{60} systems leads to fairly simple crystalline packing arrangements for the various compounds (A is an alkali metal).[11–15] The number of observed compounds is large due to the many possible valences of C_{60} molecules. Additional structure in the phase diagrams is provided by a number of transformations that have been observed with changing temperature.[10,16–22] These phase transformations and differing phase sequences found for fullerides of different alkali metals have motivated this and previous studies that refine the A_xC_{60} phase diagrams. Numerous modifications are indicated for the provisional phase diagram proposed some time ago by Zhu *et al.*[11]

In this paper, we present temperature- and stoichiometry-dependent x-ray photoelectron spectroscopy (XPS) results for the Rb and Cs fullerides in the region of the $x=1$ phases. The results are used to deduce the corresponding portions of the binary phase diagrams which, we conclude, exhibit two invariant reactions. The other alkali-metal-fulleride phases are discussed briefly, and predictions are made about the as-yet-unexplored high-temperature regions of the phase diagram. This discussion is preceded by presentation of a pure C_{60} phase diagram based on accumulated experimental and theoretical results. Finally, the formation of single-phase samples via high-temperature decomposition with fractional sublimation is discussed.[23,24]

II. EXPERIMENTAL DETAILS

The XPS measurements were performed in ultrahigh vacuum using monochromatized Al $K\alpha$ radiation ($h\nu=1486.6$ eV). C_{60} was evaporated from Ta boats and condensed onto heated GaAs(110) substrates that were cleaved *in situ*. A chromel-alumel thermocouple, attached to the sample holder, was used to monitor the temperature of samples heated radiatively by a tungsten filament. Film thicknesses from 400 to 1000 Å were used in the present studies. During C_{60} deposition, substrates were held at 450 K to facilitate the formation of highly crystalline samples.[25–27] Alkali-metal reaction was then accomplished by exposing the C_{60} films, held at 450 K, to the flux produced by SAES alkali-metal dispensers at chamber pressures in the low 10^{-10}-Torr range. Compositions were determined from XPS core-level feature intensities[28] and were checked for time dependences after alkali-metal addition. An initially decreasing alkali-metal contribution in the XPS spectrum signaled in-diffusion which saturated after $\sim$1 h for K_xC_{60} and within a few hours for Rb_xC_{60}. In-diffusion of Cs generally required >12 h of annealing to reach an equilibrated state. Extended annealing at temperatures in excess of 500 K often resulted in sublimation of fullerenes, alkali-metal atoms, or both depending on the initial composition. This

phenomenon is discussed in Sec. V. Previous studies of films prepared under similar conditions have employed scanning tunneling microscopy,[25,26] low-energy electron-diffraction,[26,27] photoemission,[27,28] and transport measurements.[29] These studies demonstrated high crystallinity and numerous indications of fulleride phase formation.

III. C_{60} PHASE DIAGRAM

In this section we focus on the behavior of pure C_{60} and assemble, in Fig. 1, an equilibrium phase diagram covering a wide range of temperatures and pressures. We mention at the outset that C_{60} is metastable with respect to the other forms of crystalline C (graphite and diamond) by ~ 0.4 eV/atom.[30] However, the kinetic barriers separating these forms are large, and transformation from one to another requires extreme temperatures or pressures. We will use the word equilibrium to describe the local free-energy minimum where C is fixed in fullerene form.

At equilibrium, solid and vapor phases of a material can coexist. Plotting the equilibrium vapor pressure against temperature gives the solid-vapor coexistence line $P(T)$. A portion of this line has been determined by Abrefah *et al.*[31] using thermogravimetric analysis. Their data are shown by solid circles in Fig. 1. The solid connecting line is their fit to $P(T)=P_0 e^{(-\Delta H/kT)}$, which can be derived from the Clausius-Clapeyron equation assuming ideal gas behavior.[32] The enthalpy of sublimation, ΔH, determined in Ref. 31 was 38 ± 1 kcal/mol (1.65 eV/molecule) in this temperature range. This compares favorably with the value derived by Pan *et al.*[33] from a Knudsen cell effusion experiment, $\Delta H = 40.1\pm1.3$ kcal/mole.

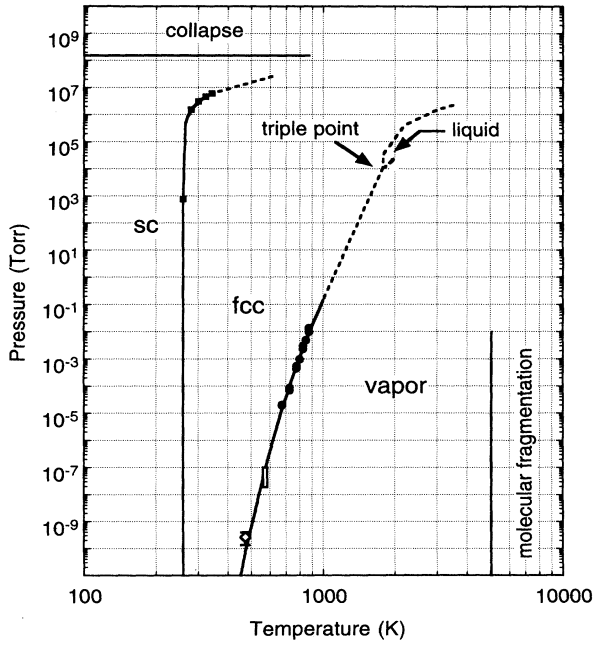

FIG. 1. Phase diagram of C_{60}. Solid lines derive from experiment, and dashed lines are theoretical or reflect extrapolations from experiment. The pressure dependence of the transition from the simple cubic phase (sc) to the face-centered-cubic phase (fcc) is from Ref. 38, and the delineation between the fcc and vapor phase is based on the results of Refs. 31 and 34 and this work. The high-temperature and -pressure regime is based on calculations from Ref. 36; the existence of a liquid phase remains to be proven. The dashed line between the calculated triple point and the solid circles is a guide to the eye. Molecular collapse and fragmentation are indicated at high pressure or high temperature.

An extrapolation of this ideal gas behavior can be expected at lower pressures. To verify this, we determined the sublimation rate of a highly crystalline (111)-oriented C_{60} film held at 473 K. The decreasing film thickness was monitored with XPS by measuring the intensity of photoelectron emission from the underlying substrate. The sublimation rate was ~ 0.5 monolayer (ML) per hour. The sublimation rate approximates the equilibrium impingement rate Γ at low pressure, so the vapor pressure can be calculated using the relationship[32]

$$\Gamma = 3.513\times10^{22}(MT)^{-1/2}P(T)\ .$$

Here Γ is in molecules $cm^{-2}\,s^{-1}$, M is the molecular mass in amu, P is in Torr, and T is in K. The resulting pressure 2.7×10^{-10} Torr is given by the open diamond in Fig. 1 at 473 K.

The results of film growth experiments reported by Hebard *et al.*[34] can also be used to give a lower bound on $P(T)$. They reported that a C_{60} source (Knudsen cell) held at 573 K resulted in film growth at a rate of 5–20 Å/min, corresponding to an impingement rate of 0.6–2.4 ML/min or a vapor pressure of $2.2-8.8\times10^{-8}$ Torr. This range is shown by a bar in Fig. 1. The result corresponds to a lower bound on $P(573\ \mathrm{K})$ because the sticking coefficient of C_{60} cannot exceed unity and because the vapor pressure at the substrate cannot exceed the Knudsen cell pressure. This result and ours are in good agreement with extrapolation of the solid-vapor coexistence line using the ideal gas relationship. We extend the curve with this form using a solid line in Fig. 1.

The existence of a liquid phase for C_{60} remains uncertain.[35] In the calculations of Cheng, Klein, and Caccamo[36] a stable liquid phase was predicted for a small region of temperature and pressure. Other calculations by Hagen *et al.*[37] suggested that liquid C_{60} will not exist in equilibrium since its free energy is always higher than that of the solid or vapor phases. Experiments have neither confirmed nor refuted the existence of the liquid phase.

The high-temperature, high-pressure portion of Fig. 1 is based on the assumption that a liquid phase does form. In this case, the solid-vapor coexistence line will terminate at a triple point, predicted to be at ~ 1775 K and ~ 14 bars (1.1×10^{4} Torr).[36] At temperatures above the triple point, a liquid-vapor coexistence line and a liquid-solid coexistence line are found. The liquid-vapor branch terminates in a critical point where the vapor and the liquid become indistinguishable. Cheng, Klein, and Caccamo[36] estimate this point to fall between 1900 and 2050 K, and it remains for experiment to investigate this behavior.

An extrapolation of the experimentally determined vapor pressure curve, assuming ideal behavior, does not intersect the calculated triple point. This may indicate a significant deviation of the vapor pressure from ideality at high temperatures or an offset in the calculated values. In Fig. 1 we use a straight dashed line to connect the calculated triple point and the experimental vapor pressure curve.

The fcc-sc (simple cubic) coexistence line, at the left of Fig. 1, defines the pressure-dependent temperature of this well-known solid-state phase transformation.[16] The filled squares are data points from Samara *et al.*,[38] who measured the transformation temperature as a function of applied pressure using differential scanning calorimetry (DSC). With no applied pressure the transformation temperature is ~260 K.[39] Since the effects of pressure below an atmosphere are negligible for solid-state transformations, we extrapolate the coexistence line toward zero pressure at 260 K. At higher pressures, the $T(P)$ relationship suggested in Ref. 38 is extrapolated with a dashed line where $dT/dp = 10.4$ K/kbar (1.4×10^{-5} K/Torr). We note that dT/dP depends upon the medium transferring the pressure since gas molecules can diffuse into the C_{60} lattice and partially negate the effects of the applied pressure. This is discussed in more detail below. The Gibbs phase rule for a single-component system at fixed pressure states that two phases can be in equilibrium only at one temperature. Hence any coexistence of the fcc and sc phases over a range of temperatures, as has been sometimes reported,[39] *must* result from a nonequilibrium phase distribution produced by cooling too rapidly or from an impurity in the sample, as discussed in Sec. IV.

The horizontal line segment at the top of Fig. 1 corresponds to the pressure limit at which destruction of C_{60} molecules has been reported.[40–43] The material produced at high pressure is interesting in its own right,[40–43] but it does not reassemble into C_{60} units when the pressure is reduced. The phase diagram in the GPa pressure regime (1 GPa = 7.5×10^6 Torr) has recently been reviewed by Núñez-Regueíro.[43] At very high temperature, the fullerenes are also expected to be destroyed. The thermal stability of an isolated molecule has been estimated by Zhang *et al.*[44] to be ~5000 K. A dashed vertical line is included in Fig. 1 to mark this predicted value. A recent calculation by Kim and Tománek[45] suggested that the molecular structure deviates from the Buckminsterfullerene isomer above about 4000 K and that molecular fragmentation can occur above ~5400 K. They point out that these temperatures are near the estimated melting and boiling points of graphite. We note that irreversible transformations do not appear on equilibrium diagrams; their presence reminds us that fullerenes are metastable.

IV. ALKALI-METAL-FULLERIDE PHASES

A tremendous amount of characterization has been performed for the alkali-metal fullerides, as reviewed recently.[46–48] Nominally stoichiometric compounds A_xC_{60} have been identified with $x=1$, 2, 3, 4, and 6.[4,10–13,18,28,49,50] Higher x values have been reported for fullerides of Na and Li.[51,52] In this section we focus on the equilibrium phase diagrams of A_xC_{60} for A = K, Rb, and Cs with emphasis on the $0<x\leq3$ region. We consider the known phases, their observed and implied coexistence regions, and their phase transformations. We delineate the behavior near the A_1C_{60} phase and, in so doing, demonstrate the existence of two invariant reactions. The compounds with higher x are considered only briefly.

Binary phase diagrams are typically meant to apply to a system at constant pressure, generally one atmosphere (760 Torr). An isobaric cut through the diagram of Fig. 1 defines the phases of pure C_{60} which appear at the left of the A_xC_{60} phase diagrams. The alkali-metal-fulleride compounds are reactive and they are generally studied under vacuum. Pressure variations below one atmosphere are expected to have negligible effects on structures and phase transformation temperatures of condensed phases. Hence data collected for equilibrium solid phases under "vacuum" conditions are applicable to atmospheric pressure phase diagrams. If the vacuum is dynamic (with pumping), the solid and vapor never reach true equilibrium since the vapor is removed as it evolves. However, slow desorption can be used to advantage for fractional sublimation, as discussed in Sec. V for temperatures well above 300 K.

A. α-C_{60}

The α-C_{60} phase appears as the leftmost region of a binary A_xC_{60} phase diagram. It is bounded by pure C_{60} and the temperature-dependent solubility limit of alkali-metal impurities in C_{60}. Phase separation occurs at higher x values. In a solid solution, the A ions are randomly distributed among the appropriate interstitial sites of the C_{60} lattice. Our photoemission work indicates that the solubility limit at 300 K is probably $x\sim0.1$ or less, and that the ions occupy octahedral sites preferentially for K_xC_{60} and exclusively for Rb_xC_{60} or Cs_xC_{60}.[17,28]

A distinction must be made between solid solutions of the fcc ($Fm\bar{3}$) and sc ($Pa\bar{3}$) structures, which we denote as α-C_{60} and α'-C_{60}, respectively. The presence of alkali-metal atoms can be expected to change the fcc-sc transformation temperature. Additionally, the two phases are likely to have different solubility limits. These factors are accounted for by the inclusion of either a peritectoid or a eutectoid transformation.[53,54] The restriction that the fcc and sc phases cannot coexist in equilibrium is relaxed by the presence of a second component (the alkali metal). Thus, coexistence of the α and α' phases can be expected over a finite temperature range below the solubility limit. For stoichiometries beyond the solubility limit, coexistence must again be limited to a single temperature.

In Fig. 2 we depict the two possibilities for the low stoichiometry region of an A_xC_{60} phase diagram. Generality is maintained by denoting the first encountered compound A_nC_{60} ($n=3$ for A = K and $n=1$ for A = Rb or Cs). The peritectoid case is depicted in Fig. 2(a) characterized by the invariant temperature T_P and composition x_P. This behavior is required when the alkali-metal atoms increase the fcc-sc transformation tempera-

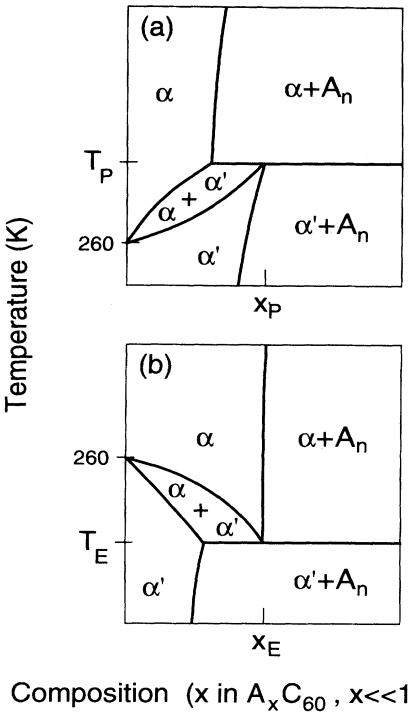

FIG. 2. A_xC_{60} binary phase diagram in the region near pure C_{60}. α and α' represent solid solutions of alkali-metal ions in the fcc and sc structures of C_{60}, respectively. Alkali-metal incorporation must raise or lower the fcc-sc transition temperature relative to that observed for pure C_{60}, namely 260 K. Panel (a) defines the peritectoid behavior required if the temperature is raised, with T_P and x_P representing the peritectoid temperature and stoichiometry. Panel (b) defines the eutectoid behavior required if the temperature is lowered, with T_E and x_E representing the eutectoid temperature and stoichiometry. A_n represents the first binary compound, A_1C_{60} or A_3C_{60}, depending on the alkali metal.

ture relative to pure C_{60}. At the composition x_P, α-C_{60} and A_nC_{60} will coexist above T_P but they will transform completely to α'-C_{60} as the temperature is lowered through T_P. Figure 2(b) shows the eutectoid case where the alkali metal suppresses the transformation temperature relative to pure C_{60}. At the characteristic composition x_E, only α-C_{60} will be present when the temperature is above the invariant temperature T_E, and there will be complete transformation into α'-C_{60} and A_nC_{60} as the temperature is lowered through T_E. For either type of transformation, a coexistence region of α-C_{60} and α'-C_{60} will be encountered for stoichiometries below the characteristic composition. Above the characteristic composition, there will be no coexistence of α-C_{60} with α'-C_{60}. Instead, one or the other will be in equilibrium with A_nC_{60}, depending on the temperature, and the transformation will be abrupt at the invariant temperature.

The variation in the transformation temperature from α-C_{60} to α'-C_{60} has not been determined for dilute doping of C_{60} with K, Rb, and Cs, but results are available for other systems. Since the fcc-sc transformation is believed to be driven by interaction of the not-quite-spherical C_{60} molecules, one might expect the temperature to be suppressed if the lattice constant were increased by impurity uptake. Indeed, the incorporation of molecular oxygen[55] or solvent molecules such as benzene or toluene[56] decreases the transformation temperature. Incorporation of small amounts of Na in C_{60} reportedly has the same effect.[57] One can crudely label this phenomenon as "oil in the gears" since the molecular "friction" is reduced by the impurity. The terms negative pressure[55] and chemical pressure[18,51] have also been used to describe the lattice expanding effect. Addition of N_2, which has a molecular size similar to O_2, seems to have no effect on the transformation temperature, an observation that is not yet understood.[55] Elevation of the transformation temperature can be expected for impurities that inhibit the rotational diffusion in the fcc phase, either sterically or through charge-transfer-induced lattice contraction. This can be thought of as "sand in the gears" since reorientation is hindered. Such a situation has been found for dilute amounts of K in C_{70} where the ordering transformation temperatures of the host C_{70} have been increased.[24] The case of O_2 incorporation in C_{60} seems to be an example of both effects since reorientation is hindered[58] yet the transformation temperature is suppressed.[55] It may be that the dynamics in the O_2-containing fcc phase are biased against the sc orientations, providing an alternate explanation for suppression of the transformation temperature. It is apparent that the direction and magnitude of the transformation temperature shift depend on the details of the impurity-host interaction. In cases where little or no charge transfer is expected, the trend is to decrease the transformation temperature. In cases where charge transfer occurs, we are aware of only the K-C_{70} and Na-C_{60} results, and these indicate opposite effects. It remains for future work to delineate the details and relative abundances of peritectoid and euctectoid systems.

B. A_1C_{60}

The filling of all of the octahedral sites of the fcc C_{60} lattice, while maintaining cubic symmetry, results in A_1C_{60} in the rocksalt (NaCl) crystal structure. This structure has been reported for the fullerides of K, Rb, and Cs at high temperatures.[18,22,50] A_1C_{60} is also stable at room temperature[28] for A =Cs or Rb, but the 300-K structures are noncubic.[18,22] It has been demonstrated that K_1C_{60} undergoes a eutectoid transformation into α-C_{60}+K_3C_{60} upon slow cooling to below 425 K.[10,17,59] Thus K_1C_{60} exists only as a metastable phase below this temperature.[17,60] When monitored with XPS, the $K_1C_{60}\rightarrow\alpha$-$C_{60}$+$K_3C_{60}$ transformation is accompanied by drastic changes in the line shape of the K 2p core-level emission. These line-shape changes indicate the diffusion of K ions from octahedral sites of K_1C_{60} (to leave regions of the sample that are α-C_{60}) into tetrahedral sites, thus nucleating grains of K_3C_{60} with complete filling of tetrahedral and octahedral sites. For the Rb- and Cs-C_{60} systems, the phase transformation involves a lattice dis-

tortion with no major redistribution of the alkali-metal sublattice. While the spectral changes accompanying these transformations are far more subtle, they are still observable with high precision XPS.

In Fig. 3(a) we show Rb 3*d* core-level spectra for a Rb_1C_{60} sample measured at 300 and 480 K to bracket the transformation temperature. A single spin-orbit doublet is present at both temperatures, indicating a single type of coordination for Rb ions in each structure. However, a shift of the spectral features accompanies the phase transformation, indicating that the Madelung energies and screening properties of the two phases differ. The binding-energy shift occurs abruptly at the phase transformation, in contrast to a continuous shift that might be expected to result from thermal expansion of the lattice. The abruptness of the transformation is emphasized in Fig. 3(b), where the Rb 3*d* binding-energy shifts obtained by least-squares peak fitting are plotted versus temperature for a cooling and heating cycle. To obtain the plot, the sample heater current was decreased (or increased) at ~30 min intervals to give an overall temperature ramping rate of ~0.2 K/min. Substantial thermal hysteresis was observed as the transformation was reversed for ramping rates in the 0.2–2.0-K/min range. The hysteresis and the finite temperature interval over which the phase transformation is observed introduce ambiguity when defining the transformation temperature. Here we will use the binding-energy shift *onset* measured upon heating to define the transformation temperature. We thus arrive at a value of 405 K for $x = 1.0$.

To fully characterize the phase transformation, data points must be taken at stoichiometries above and below $x = 1$. We therefore examined samples with $x = 0.2$ and 0.5 which consisted of Rb_1C_{60} in equilibrium with an appropriate amount of α-C_{60}. The α-C_{60} contains a negligible amount of Rb and therefore the Rb 3*d* spectra for $x = 0.2$ and 0.5 were identical to that shown for Rb_1C_{60} in Fig. 3(a). Phase coexistence can be confirmed by decomposition of the C 1*s* line shape, as shown in Fig. 4(a), into a sharp α-C_{60} peak and a broader, shifted Rb_1C_{60} peak.[28] Binding-energy shifts measured for the $x = 0.2$ and 0.5 samples are shown in Figs. 4(b) and 4(c). Identical transformation onset temperatures are found, consistent with phase-separated Rb_1C_{60} (with the same composition and therefore the same chemical potential) in both samples. This is independent evidence of phase separation corroborating the line-shape analysis of Fig. 4(a). These results are inconsistent with the model proposed by Zhu *et al.*,[11] where a solid solution extends

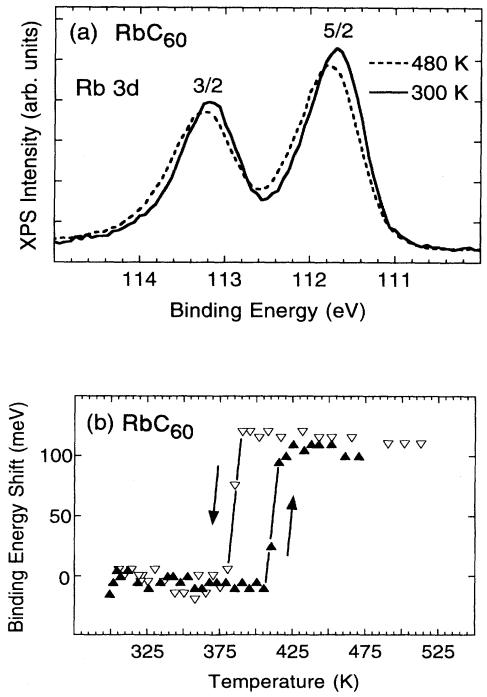

FIG. 3. (a) Rb 3*d* core-level spectra for Rb_1C_{60} at temperatures above and below the phase transformation. The rigid shift in binding energy reflects a change in the electrostatic potential for the Rb ions in the interstitial site as the lattice undergoes a cubic to noncubic distortion. (b) summarizes the Rb 3*d* core-level binding energies that were measured as a function of temperature. The abrupt change identifies the phase transformation.

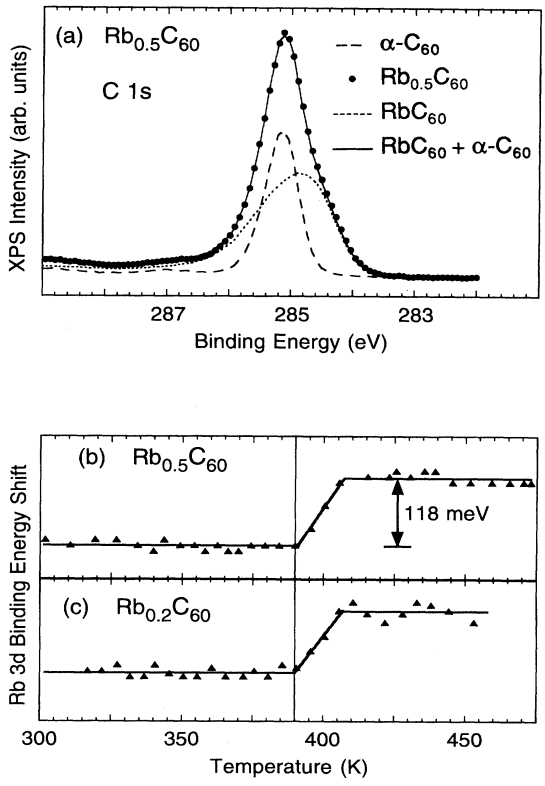

FIG. 4. (a) C 1*s* photoemission spectrum of $Rb_{0.5}C_{60}$ (data points) decomposed into contributions from Rb_1C_{60} and α-C_{60} (broken lines). The solid line is the sum of the two contributions. (b) and (c) summarize the binding-energy shifts of the Rb 3*d* feature measured for samples with global stoichiometry $Rb_{0.5}C_{60}$ and $Rb_{0.2}C_{60}$. Identical transformation onsets for both stoichiometries confirm phase separation into α-C_{60} and Rb_1C_{60}, as suggested by the C 1*s* decomposition of (a).

from $x=0$ to 1. In such a solid solution, we would expect a shift in the transition temperature for a change by a factor of 2.5 in the Rb content.

For $1<x<3$, phase separation between Rb_1C_{60} and Rb_3C_{60} is found. An accompanying change in the transformation temperature is expected because this Rb_1C_{60} corresponds to the high stoichiometry limit of the "1" phase field (the Rb_1C_{60} that is in equilibrium with α-C_{60} corresponds to the low stoichiometry limit). As will be discussed below, the chemical potential varies with x across the phase field. To examine the stoichiometry range $1<x<3$, we prepared a sample with $x=1.5$. The Rb 3*d* spectrum shown in Fig. 5(a) can be well described by adding scaled spectra from Rb_1C_{60} and Rb_3C_{60} samples.[28] Three clear peaks, labeled *A*, *B*, and *C*, result from the overlapping contributions from Rb ions in tetrahedral and octahedral sites. The line-shape decomposition shows that peaks *A* and *B* have a Rb_1C_{60} contribution while peak *C* arises strictly from the Rb_3C_{60} portion of the sample. Figure 5(b) shows the binding energies of these peaks measured as a function of temperature, where it can be seen that peaks *A* and *B* exhibit the binding-energy shift expected for Rb_1C_{60}. Lines through the data points for *A* and *B* are a guide to the eye. In contrast, peak *C* shifts continuously. This would be expected for lattice expansion within a single phase, in this case Rb_3C_{60}. The curve through the data points for peak *C* is a calculation of the photoelectron binding-energy shift expected for a tetrahedral ion as a result of the lattice expansion of Rb_3C_{60} (see Sec. IV C for details). The transformation onset at ~405 K is identical within experimental error to that measured for $x=1.0$. The composition of our $x=1.0$ sample, therefore, likely represents the high stoichiometry limit of the Rb_1C_{60} phase field.

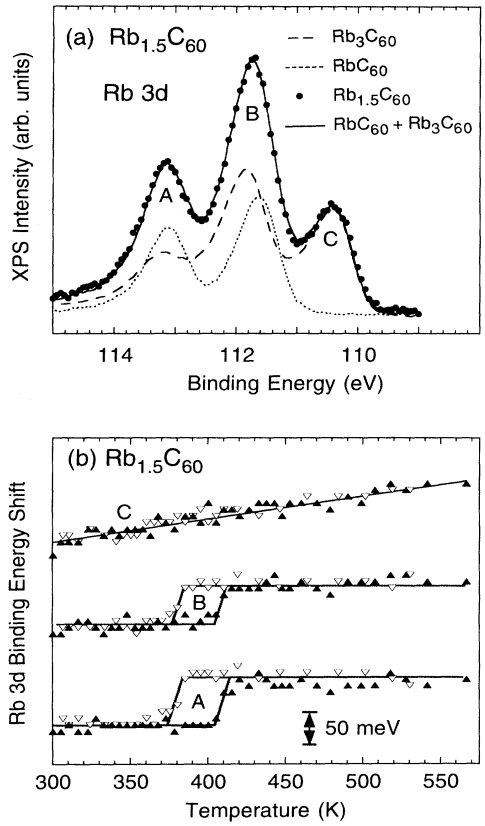

FIG. 5. (a) Rb 3*d* photoemission spectrum of $Rb_{1.5}C_{60}$ (data points) decomposed into contributions from Rb_1C_{60} and Rb_3C_{60} (broken lines). The solid line is the sum of the two contributions. A single Rb 3*d* spin orbit doublet appears for Rb_1C_{60} because all of the ions are in equivalent octahedral sites. Two overlapping doublets are seen for Rb_3C_{60} because inequivalent tetrahedral and octahedral sites are occupied and their 3*d* features are offset by 1.2 eV. (b) Binding-energy shifts of features *A*, *B*, and *C* of (a) measured during a temperature cycle. Hysteresis loops for *A* and *B* support the phase separation indicated in (a). These components have Rb_1C_{60} character. Lines through the data for *A* and *B* are a guide to the eye. The curve through the data points for *C* is the result of a calculation that describes the effects of lattice expansion on the binding energy for Rb_3C_{60}.

For Rb_1C_{60}, experimental results demonstrate single-phase material at 480 and 300 K.[18,21,28] Constructing a phase diagram with the appropriate phase fields requires at least *two* invariant transformations. This is illustrated in the proposed Rb_xC_{60} phase diagram of Fig. 6, where eutectoid and peritectoid transformations are connected by a two-phase region. This is a common motif for systems that exhibit ordering transformations, and equivalent topologies are found for β-brass[53] (Cu-Zn), η-bronze[53] (Cu-Sn), and stage-2 Li-intercalated graphite.[61] The rocksalt structure is denoted 1 and the noncubic structure is denoted 1′. The adjacent Rb_3C_{60} phase boundary is not shown in Fig. 6, but its presence is indicated in the two-phase regions (Rb_3C_{60} is abbreviated 3). The 1 phase is shown to transform at the eutectoid temperature into the 1′ structure and a small amount of α-C_{60}. The 1′ phase transforms upon heating to the 1 phase

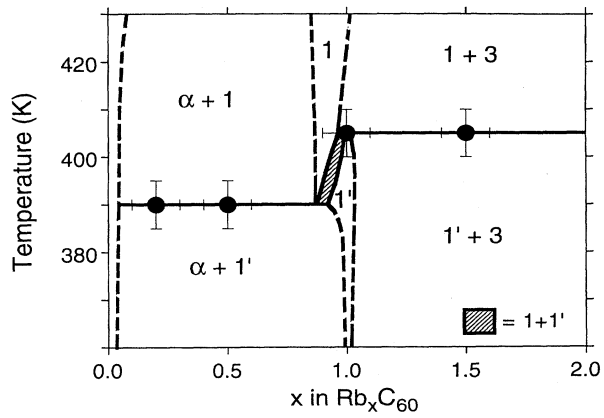

FIG. 6. Proposed Rb_xC_{60} binary phase diagram in the region of Rb_1C_{60}. Data points are derived from Figs. 4 and 5, as described in the text. The shaded region shows coexistence for the 1 and 1′ phases. Cooling a pure 1 sample through the eutectoid temperature of 390 K would produce two new phases α and 1′. Heating a pure 1′ sample through the peritectoid temperature of 405 K would produce two new phases 1 and 3. Phase boundaries are schematic as indicated by the dashed lines.

and a small amount of Rb_3C_{60} via a peritectoid transformation. Coexistence of the 1 and 1′ phases will occur over a finite temperature range. The compositions of the phase boundaries are not yet known precisely, as implied by the dashed lines of Fig. 6, and further studies are needed to define the widths of the phase fields.

The peritectoid and eutectoid temperatures of 405 and 390 K drawn in Fig. 6 can be compared to the transformation temperatures obtained in other work on Rb_xC_{60}. The transformation onset reported by Janossy *et al.*[20] for an $x=2$ sample was ~400 K. Differential scanning calorimetry data reported by Zhu *et al.*[18] for an $x=1.4$ sample showed an extended transformation consisting of a broad "precursor" and a comparatively sharp peak, with onsets at ~345 and ~410 K, respectively. The peak is in good agreement with our results, while the precursor feature may be due to transformation of metastable structures, that were quenched upon cooling, to the equilibrium 1′ structure. The infrared absorption measurements of Martin *et al.*[19] showed a transformation onset at ~375 K for a film of unknown composition but with a large fraction of Rb_1C_{60}. In poorer agreement, coexistence of the 1 and 1′ phases between 295 and 350 K was reported by Tykco *et al.*[21] based on NMR spectroscopy for a sample that was reported to be pure phase. This suggests that the transformation upon cooling may not be complete due to quenching or contamination in powder samples. In subsequent NMR work with a $Rb_{0.6}C_{60}$ sample, the phase transformation was measured with a cooling onset of ~390 K (in better agreement with our results), although a small amount of the high-temperature phase was detected below room temperature.[62]

The phase diagram of Fig. 6 has important implications for equilibrium samples. First, it indicates that complete conversion from pure 1 to pure 1′ will occur over a range of temperature (~15 K) because of the region of coexistence. This will occur only for x very near 1. The sharpest transformations should be measured in two-phase samples at stoichiometries below x_E or above x_P. Thus nonstoichiometric, but equilibrated, samples are valuable for defining transformation temperatures. Second, the demonstration of two transformation temperatures T_E and T_P implies a finite width for the 1 and 1′ single-phase regions. The width could be provided by octahedral site Rb vacancies on the low-x side and perhaps by tetrahedral site Rb interstitials on the high-x side. This is significant because none of the compositional phase boundaries have been determined with precision for the alkali-metal fullerides. Finally, it is important to realize that any sample containing more than two phases must reflect nonequilibrium character or result from contamination, either of which will affect properties such as transformation temperatures.

Studies analogous to those discussed for Rb_xC_{60} have been performed for Cs_xC_{60}. Binding-energy shifts of the Cs 4*d* core-level XPS features are plotted in Fig. 7 for three compositions near $x=1$. The measured transformation onsets are 345, 390, and 410 K for $x=0.8$, 1.0, and 1.3, respectively. The trend to increased transformation temperatures as the stoichiometry crosses $x=1$ is

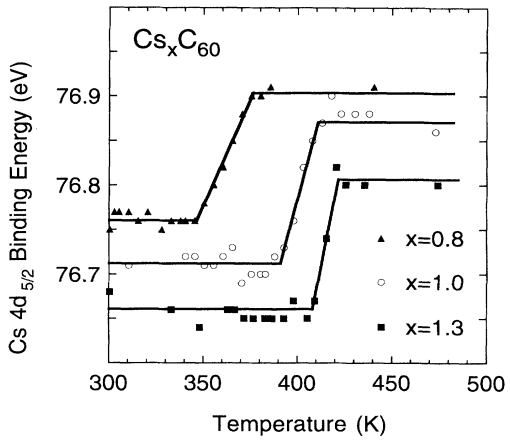

FIG. 7. Binding energies of the Cs $4d_{5/2}$ core-level features measured as a function of temperature for Cs_xC_{60} at the compositions indicated. Data points shown for the heating part of the cycle reveal that the transformation temperature is composition dependent. These results form the basis for the phase diagram in Fig. 8 for Cs_xC_{60}.

the same as that observed for Rb_xC_{60}. We suggest a similar topology for the Cs_xC_{60} phase diagram, as drawn in Fig. 8. Since Cs_3C_{60} is not stable in the temperature range studied, the 1 and 1′ phases are in equilibrium with Cs_4C_{60} for $1<x<4$. This difference will affect the solubility limit of alkali-metal interstitials for x just beyond 1; i.e., the $x=1$ phases will extend to $1+\delta(T)$, and $\delta(T)$ may vary considerably from Rb_1C_{60} to Cs_1C_{60}. The alkali ion size will, of course, also play a role in determining this phase boundary as well as the low-x phase boundary $1-\varepsilon(T)$. The width of the phase field $(\varepsilon+\delta)$ will in turn

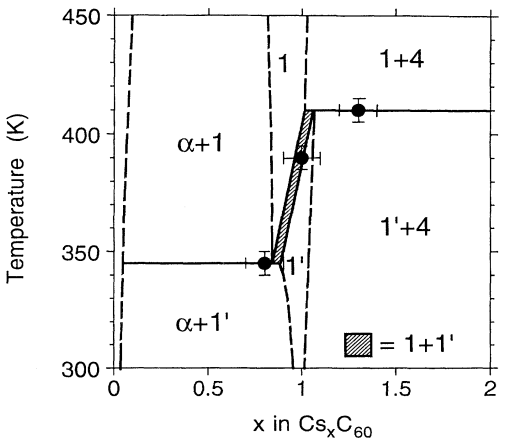

FIG. 8. Proposed Cs_xC_{60} binary phase diagram in the region of Cs_1C_{60}. Data points are derived from Fig. 7. As for Rb_xC_{60}, there are two invariant reactions, namely a peritectoid at 345 K involving $1\rightarrow\alpha+1'$ and an eutectoid at 410 involving $1'\rightarrow 1+4$. Coexistence of 1 and 1′ is indicated by the shaded region. Phase boundaries are schematic as indicated by the dashed lines.

influence the difference between eutectoid and peritectoid temperatures which is found to be considerably larger for Cs_xC_{60}, suggestive of a wider field.

From the data in Fig. 7, we can place an upper limit on T_E of 345 K and a lower limit on T_P of 410 K. Notice that in the XPS results, each measured transformation is fairly narrow (<30 K). The 65-K span between T_P and T_E compares well to the transformation range in the DSC results of Zhu *et al.*[18] NMR results of Tycko *et al.* also indicated a transformation range of temperatures much broader than observed in each individual experiment here.[21] This may indicate a distribution of stoichiometries in the powder samples employed for those measurements, since inhomogeneity would result in a broad transformation with temperatures bracketed by T_E and T_P. Such inhomogeneity is not difficult to envision since the diffusion of Cs into C_{60} is sluggish, and concentration gradients can be expected for large grains in a powder sample.

C. A_3C_{60}

The A_3C_{60} structure, for A =K or Rb, is produced by filling all the tetrahedral and octahedral sites of the fcc C_{60} lattice.[12–15] NMR studies have suggested that there is a phase transformation for A_3C_{60}, wherein tetrahedrally coordinated alkali-metal ions become inequivalent at low temperatures.[63,64] The transformation temperature is reported to be 370 K for Rb_3C_{60} and 210 K for K_3C_{60}. The physical nature of this transformation remains unknown, and other techniques have thus far been unable to distinguish the inequivalent tetrahedral ions.

In Fig. 9 we show the Rb 3*d* photoemission spectrum of a Rb_3C_{60} sample prepared by decomposition reaction together with the measured binding-energy shifts of the three spectral peaks, labeled *A*, *B*, and *C* as in Fig. 5. We see no abrupt shifts and find no discernible evidence for a phase transformation. Instead, the lines superimposed on the data points of Fig. 9(b) show the behavior associated with lattice expansion. These shifts were calculated assuming a lattice of point charges, taking into account a Madelung term, a screening term, and a constant offset.[65] A small correction due to Pauli repulsion of nearest-neighbor ions was neglected. The Madelung term describes the changing electrostatic potential at the ion site as the lattice expands. This term varies as the reciprocal of the lattice constant, a_0, and can be derived from the Evjen sums calculated by Zhang, Zheng, and Benneman[66] and the lattice constant versus temperature data of Zhou *et al.*[50] The screening term describes the final-state relaxation wherein neighboring molecules polarize toward the photohole to lower the energy of the system and decrease the binding energy of the photoelectron. For this term we simply sum nearest-neighbor contributions using the form suggested by Lof *et al.*[67] for pure C_{60}, which varies as a_0^{-4}. We use the polarizability for C_{60}^{3-} calculated by Quong and Pederson.[68] The final term is the binding energy of the electron in the isolated ion which is approached as the lattice constant goes to infinity and the other terms vanish. We treat this term as an adjustable parameter to normalize to the data at 300 K. The number of adjustable parameters could be reduced to zero given the work function of Rb_3C_{60} and the 3*d* binding energy in the isolated Rb^- ion. The calculated response is in good agreement with the data over the 400-K range examined.

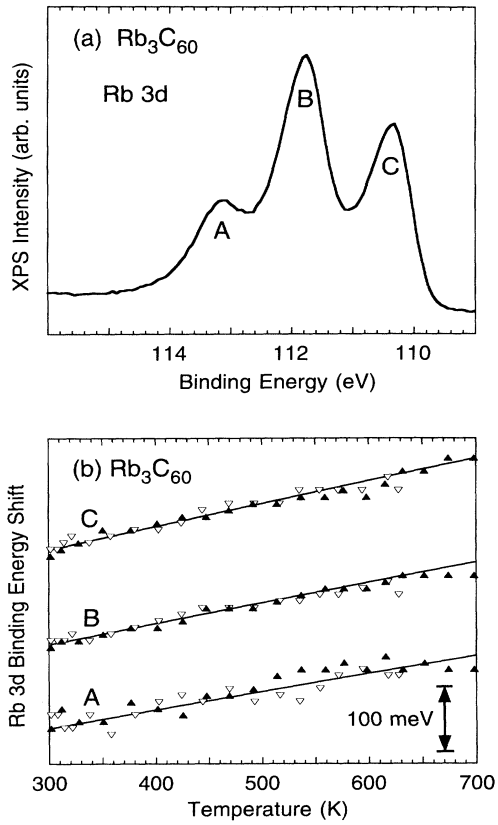

FIG. 9. (a) Rb 3*d* photoemission spectrum for Rb_3C_{60}. The two chemical environments for Rb ions in Rb_3C_{60} produce two spin-orbit split doublets, offset by 1.2 eV. *C* corresponds to the $3d_{5/2}$ component of the tetrahedral ions, *A* is dominated by the $3d_{3/2}$ component of the octahedral ions, and *B* is derived from $3d_{3/2}$ (tetrahedral) and $3d_{5/2}$ (octahedral) emissions. (b) The binding energy shift of the Rb 3*d* features measured during a temperature cycle. Lines through the data are calculated shifts based on the lattice expansion of Rb_3C_{60}, as discussed in the text. The absence of a step at 405 K indicates that there was no discernible amount of Rb_1C_{60}.

D. A_xC_{60} ($x>3$)

The incorporation of K or Rb ions beyond $x=3$ is accompanied by a change in the C_{60} lattice from fcc to bct (body-centered-tetragonal) for the $x=4$ phase.[11–13] Incorporation of Cs beyond $x=1$ also produces this phase since the $x=3$ phase does not form under equilibrium conditions, at least in the temperature range explored to date.[12,28] Decomposition reaction studies, discussed below, have demonstrated that Cs_4C_{60} is the most stable of the Cs_xC_{60} compounds, and the same is expected for K_4C_{60} and Rb_4C_{60}.

K, Rb, or Cs incorporation beyond $x=4$ results in formation of A_6C_{60} that is based on a bcc fullerene lattice with six equivalent tetrahedral sites per fullerene.[11–13] The lattice constant of Rb_6C_{60} can be reduced significantly when the overall composition is less than $x=6$,[11,60] a fact attributed to Rb vacancies. The most direct measurement of the phase boundary described so far suggests that the "solubility limit" of such vacancies at 523 K is 0.4 per C_{60}, resulting in $Rb_{5.6}C_{60}$ at 523 K in equilibrium with Rb_4C_{60}.[60]

Sodium incorporation beyond $x=3$ results in multiple occupation of the octahedral site as the fcc structure is maintained. Sodium uptake has been reported to yield stoichiometries as high as ~ 9.[51] A solid-state electrochemical experiment has also suggested that up to 12 Li ions per molecule can be incorporated in a C_{60} electrode.[52] Similar solid-state phases have not been reported for reaction with the heavier alkali metals. However, it has been shown that fullerene molecules adsorbed on alkali-metal surfaces will take on more than six electrons.[24,27] Finally, we note that nothing has been reported about the solubility of C_{60} in the various alkali metals, leaving the metal side of each phase diagram undetermined. One might assume that the strong tendency to exchange charge would result in favorable Madelung potential contributions to stability. This would raise the melting and boiling temperatures of the solid solutions relative to the pure alkali metals and would result in peritectic transformations.

E. Proposed fulleride phase diagram at high temperature

The known fulleride phase behavior up to about 800 K and the results of our thermal decomposition experiments make it possible to propose a complete phase diagram. Following convention, we will discuss the phase diagram at one atmosphere. From Fig. 1, the sublimation point for C_{60} at 1 atm is ~ 1500 K, and no liquid phase is expected at any temperature (this remains to be proved). For the alkali metals, the melting points at 1 atm are 336, 312, and 301 K for K, Rb, and Cs, and their respective boiling points are 1033, 959, and 942 K.[69] The large gains in cohesive energy associated with fulleride formation[30] suggest that their melting and/or vaporization temperatures will be much higher than for the alkali metals or C_{60}.

The K-C_{60} phase diagram, shown in Fig. 10, includes $x=1$, 2, 3, 4, and 6 phases as well as solid solutions of K in C_{60} and C_{60} in K. We can use it as a prototype for the other fullerides, with obvious differences that must be introduced for Rb and Cs because of the behavior near $x=1$, as discussed above, and the absence of the $x=3$ phase for Cs. (It is possible that a Cs_3C_{60} phase is stable at elevated temperatures, but there are no data to define the temperature region of stability.) For K-C_{60}, the temperatures of reported transformations are indicated in the figure, while undetermined temperatures of predicted transformation are labeled T_1-T_8. We predict that the sc-to-fcc transformation temperature will be increased from 260 K by dilute K addition, resulting in a peritectoid transformation [see Fig. 2(a) for details]. The invariant temperature T_1 is not known. The first nominally stoichiometric phase K_1C_{60} is stable above a eutectoid temperature of 425 K.[17] The presence of this phase, which is not predicted to be particularly stable by simple electrostatic models,[7] appears to be related to rotation of the C_{60} molecules which alters the relative position of the free-energy minima for α-C_{60}, K_1C_{60}, and K_3C_{60}. We suggest that thermal expansion, which reduces the Madelung energy, will eventually make this phase unstable at higher temperatures and that it will transform to K_3C_{60} and α-C_{60} at some temperature T_2. This behavior is an alternative to our previous suggestion[17] that K_1C_{60} would join the α-C_{60} phase field above a miscibility gap. The K_1C_{60} phase field is drawn extending below $x=1$, reflecting the likelihood of K vacancies when the phase is in equilibrium with α-C_{60}. A similar extension is not

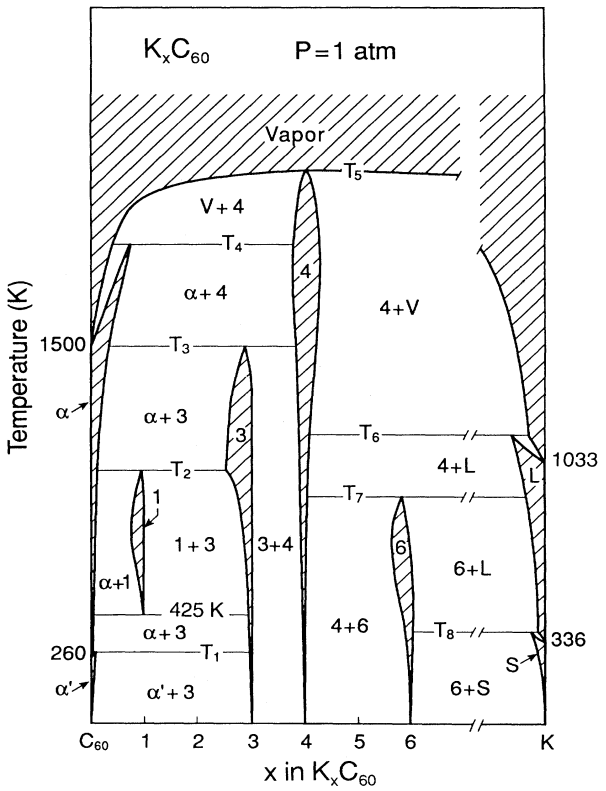

FIG. 10. Proposed phase diagram of K_xC_{60} extending to high temperature. Experimentally determined temperatures are indicated, while unknown temperatures of predicted transformations are labeled T_1-T_8. Underlying assumptions are that there is no liquid phase and that dilute amounts of K in C_{60} will raise the solid to vapor transformation temperature, producing a peritecticlike reaction at T_4. This is plausible because of the contribution to the cohesive energy associated with ionic bonds. The phase fields of K_1C_{60}, K_3C_{60}, K_4C_{60}, and K_6C_{60} are drawn schematically since the widths remain to be determined. Areas of two phase coexistence for equilibrium samples are shown. The stability of K_4C_{60} exceeds that of the other fullerides, based on the decomposition experiments discussed in the text. The behavior for C_{60} in solution in K(S) and K(L) is assumed to raise the S-L and L-V transformation temperatures relative to pure K.

drawn for $x > 1$ since this would require the presence of tetrahedral K interstitials which we anticipate to be less likely.

It has been speculated that the K_3C_{60} phase will join with α-C_{60} or K_1C_{60} above a miscibility gap.[11,17] Coexistence of K_1C_{60} and K_3C_{60} has been observed at the highest temperatures tested so far, ~900 K, thus placing a lower bound on the top of a miscibility gap or on the peritectoid temperature T_2.[70] Here we present an alternative prediction for the high-temperature limit of the K_3C_{60} phase field. We draw a peritectoid transformation where K_3C_{60} transforms to α-C_{60}+K_4C_{60} at T_3. This assumes that T_3 is below T_4, the sublimation temperature of α-C_{60} at its solubility limit. The instability of K_3C_{60} at high temperatures could also result from lattice expansion effects. Vibrationally excited K ions in tetrahedral sites might expand the K_3C_{60} lattice until it becomes unstable against a partitioning into α-C_{60} and K_4C_{60}, which has interstices that are large in comparison to the K_3C_{60} tetrahedral sites.

K_4C_{60} is stable at all tested temperatures. Our decomposition reaction experiments suggest that it will be the last solid phase present at very high temperature.[23] It will then coexist with a C_{60} vapor bearing a small amount of K above T_4 and it will melt or sublime congruently, starting at T_5. Heating K_6C_{60} may result in transformation at T_7, to produce K_4C_{60} and a K liquid bearing a small concentration of C_{60}, as drawn in Fig. 10. If T_7 is higher than T_6, then K_6C_{60} would transform to K_4C_{60} and K vapor. A third possibility is that K_6C_{60} may join K_4C_{60} above a miscibility gap. For this to occur, the bct and bcc structures of K_4C_{60} and K_6C_{60} must distort with increasing temperature, so that they would have the same crystal symmetry at the top of the miscibility gap.

To the best of our knowledge, the right side of the phase diagram, where fullerenes are dispersed in K, has not been investigated. The boiling and melting points of K will either be elevated or suppressed by C_{60} impurities to the temperatures T_6 and T_8. Here again, we have assumed peritectic behavior, but it remains to be seen if peritectic or eutectic transformations are found. Since it is not known whether liquid K supports an appreciable solubility of fullerenes, the solubility line of Fig. 10 is suggestive only. If the solubility is low, then heating K_6C_{60} above T_7 would produce essentially pure liquid K and K_4C_{60}. If the solubility is high, extending out to the region of fulleride compounds, then some of the fulleride phases would melt at high temperatures. The long range of the Coulomb attraction between ions might stabilize molten fullerides even though C_{60} is not expected to have a liquid phase at this pressure. At sufficiently high temperatures a homogeneous vapor of K and C_{60} is expected for all x.

Phase diagrams for Rb_xC_{60} and Cs_xC_{60} will require modifications to account for the 1′ phase, as depicted in Figs. 6 and 8. The ordering transformations suggested by NMR (Refs. 63 and 64) for K_3C_{60} and Rb_3C_{60} could also be added to show a low-temperature 3′ phase that would coexist with α' and 4. The 3→3′ phase transformation should be similar in topology to that described for the 1→1′ transformations. It is hoped that this provisional phase diagram will serve as a guide for future studies and will stimulate work that either confirms the proposed topologies or provides required corrections.

V. PHASE-PURE FULLERIDE PRODUCTION

Fleming *et al.*[12] reported that "thermal deintercalation" of K from K_6C_{60} could produce single-phase K_4C_{60}. As we subsequently demonstrated,[23] this is one example of numerous decomposition reactions that can be employed to obtain phase-pure fullerides. We have used the term distillation to describe these reactions[23,24] because of the analogy to the process for separating liquid mixtures. It is important to point out that the decomposition reaction for a fulleride of low stoichiometry will result in the loss of fullerene molecules *not* alkali-metal atoms.

In our decomposition reactions with a fulleride, the sample is heated in dynamic vacuum to a temperature where the composition is changed by fractional sublimation. When taken to completion, the composition is very near an integer stoichiometry. As an example of the application of this technique, Fig. 11 shows results for a sample of starting composition $K_{0.7}C_{60}$ that was heated at 495 K. Room-temperature XPS spectra were acquired before heating (labeled 1) and after heating for 6 and 24 h (labeled 2 and 3). The K 2*p* core-level signature shown at the left is that of K_3C_{60} in all cases because the data were acquired at room temperature. The corresponding C 1*s* spectra showed dramatic changes because the C 1*s* signal

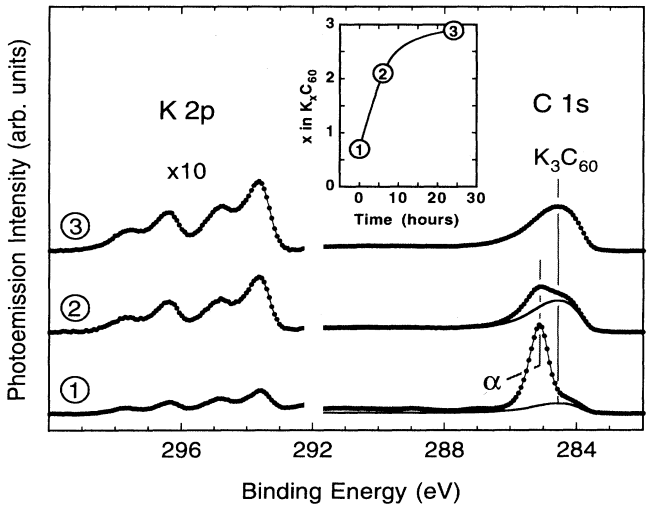

FIG. 11. Illustration of the process for production of K_3C_{60} from a sample of starting composition $K_{0.7}C_{60}$, i.e., a sample that is about 23% K_3C_{60} and 77% α-C_{60} at 300 K. The decomposition temperature was 495 K. The spectra, acquired at 300 K, show the growth of the K 2*p* feature relative to the C 1*s* emission as C_{60} molecules are desorbed. The C 1*s* feature is composed of α-C_{60} and K_3C_{60} contributions initially, but the α-C_{60} portion disappears as K_3C_{60} is approached. The inset shows the experimentally determined x values in K_xC_{60} in the as-grown sample, and after heating for 6 and 24 h.

was dominated initially by an α-C_{60} component but it evolved into the K_3C_{60} spectrum. Line-shape analysis reveals the α-C_{60} and K_3C_{60} contributions, as shown, and the composition determined by XPS is indicated in the inset. Independently, the substrate emission was monitored and this demonstrated a decrease in the film thickness due to loss of C_{60}, commensurate with the change in composition.

Results equivalent to those of Fig. 11 have been obtained for the K, Rb, and Cs fullerides of C_{60} and for the K fullerides of C_{70}. Table I summarizes studies performed to date. The first column lists starting compositions, the middle lists ending compositions, and the last gives the temperatures used to effect the change. In all cases, the decomposition reactions proceeded toward $x=4$ and, for this reason, we conclude that A_4C_{60} is the most thermally stable compound (Fig. 10). Since compositional evolution depends on fractional sublimation, the time required to complete the process depends on the bulk to surface ratio of the sample, as discussed in Ref. 23. Experience has indicated that sublimation of C_{60} from Rb_1C_{60} or Cs_1C_{60} is accompanied by the desorption of alkali-metal atoms. Accordingly, the starting films must be sufficiently thick to compensate for this. In contrast, sublimation of alkali-metal atoms from A_6C_{60} is accomplished with very little sublimation of fullerenes. As explained below, these desorption processes are a consequence of thermodynamics, and differences in chemical potentials from one system to another are reflected by the vapor-phase stoichiometries.

Several points should be noted about preparing samples by a decomposition reaction. First, the addition of Rb to a fullerene film to produce Rb_1C_{60} is often accompanied by nucleation of Rb_3C_{60} before the composition $x=1$ is reached. Once formed, it is difficult to transform this metastable phase without desorbing Rb_1C_{60}. Fortunately, the nucleation of Rb_3C_{60} can be avoided by limiting the initial composition to a low value like $Rb_{0.5}C_{60}$.

TABLE I. Summary of decomposition experiments performed to produce phase-pure fullerides. The first column lists starting compositions which represent single- or two-phase samples. The middle column lists the ending, single-phase composition after the sample is held at the temperature in the last column for a sufficient amount of time.

Starting composition	Ending composition	Temperature
K_xC_{60}, $x<3$	K_3C_{60}	495 K
K_xC_{60}, $x=6$	K_4C_{60}	650 K
Rb_xC_{60}, $x<1$	Rb_1C_{60}	515 K
Rb_xC_{60}, $x\sim2.8$	Rb_3C_{60}	620 K
Rb_xC_{60}, $x=6$	Rb_4C_{60}	675 K
Cs_xC_{60}, $x<1$	Cs_1C_{60}	495 K
Cs_xC_{60}, $x=1$	Cs_4C_{60}	650 K
Cs_xC_{60}, $x=6$	Cs_4C_{60}	700 K
K_xC_{70}, $x<1$	K_1C_{70}	495 K
K_xC_{70}, $x=1$	K_3C_{70}	575 K
K_xC_{70}, $x=3$	K_4C_{70}	635 K
K_xC_{70}, $x=6$	K_4C_{70}	650 K

The same technique can be used to prevent premature formation of K_4C_{60} when attempting to produce K_3C_{60}.[71] Second, it has been difficult to produce phase-pure A_4C_{60} by the addition of alkali metals to fcc C_{60}. In many experiments the addition of alkali-metal atoms past a composition of A_3C_{60} results in nucleation of the bcc A_6C_{60} structure.[8–10] The decomposition reaction, which approaches A_4C_{60} from a fully doped A_6C_{60} bcc structure, is preferable, as x-ray-diffraction studies have shown for powders[12] and Raman spectroscopy studies have shown for films.[72]

Decomposition with fractional sublimation can be understood by considering the thermodynamic activities of the fullerenes and the alkali metals.[73] When the vapor-phase portion of a system behaves ideally, then the activity can be defined as $a_i(x,T)=P_i(x,T)/P_0(T)$ where P_i is the partial pressure of component i for stoichiometry x and temperature T and P_0 is the equilibrium vapor pressure above the pure substance at that temperature. The chemical potential can be expressed as $\mu_i(x,T)=\mu_0+\ln a_i(x,T)$, where μ_0 represents the standard state. Raoult's law for an ideal solution of A and B then dictates that $a_B=x_B$, where x_B is the mole fraction of B.[33,73] Thus the partial vapor pressure of B above the solution is reduced as A units replace B units. Conversely, the amount of B in the vapor phase increases as the solid becomes enriched in B.

An ideal solution model is inappropriate for alkali-metal-fulleride systems because compounds are formed. In this case, the chemical potentials must be equal for coexisting compounds and they will remain constant for x values between the boundaries of the two compounds. The argument applies to both components A and B, so that a_A and a_B are constant in this range. As a result, the vapor above a two-phase sample will have a constant ratio of A to B, regardless of the relative amounts of the two compounds present. Since the vapor-phase composition will be different from the global stoichiometry, the composition of the solid will change slightly if the temperature is high enough to promote sublimation. If the vapor is removed and the system is allowed to reequilibrate, the composition of the solid will change again. In a decomposition experiment, the vapor is continually removed so that the composition of the solid changes until a stoichiometry is reached at which the vapor pressure is greatly reduced or the stoichiometry of the vapor equals that of the solid. Either option is possible only when a single-phase boundary is reached. Within a single-phase region the vapor composition and pressure can both change with x. Accordingly, a decomposition reaction will terminate within a single-phase region.

We illustrate this graphically in Fig. 12 for hypothetical materials A and B that form a compound AB.[73] The dilute solutions of B in A and A in B are denoted α and β, respectively. The compound AB exhibits slight deviations from a 1:1 stoichiometry as shown in the phase diagram in Fig. 12(a). The composition is given as the molar fraction of component B, x_B. Figure 12(b) depicts the free-energy curves for the three phases at the temperature labeled T_1 in Fig. 12(a). The free energies are plotted as a difference ΔG from those of the pure materials. Dilute

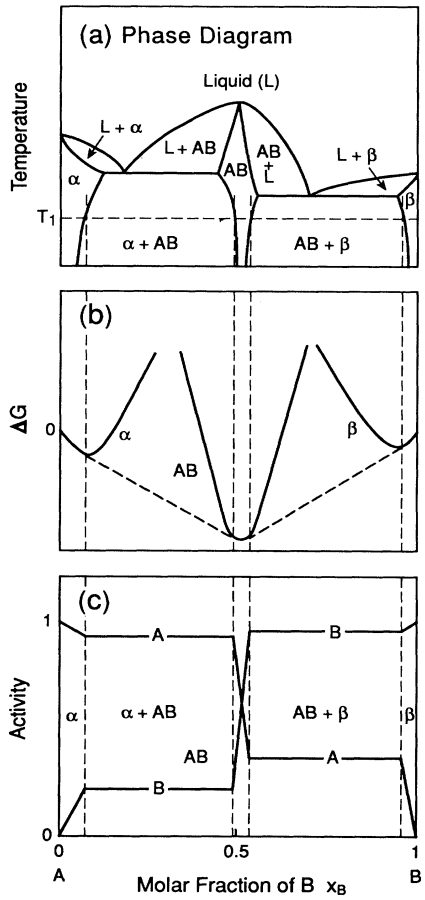

FIG. 12. (a) Hypothetical temperature-composition phase diagram for materials A and B, (b) free energies of the phases, and (c) activities of components A and B. The free-energy change in the two phase regions has a constant slope (dashed tie lines) and, therefore, the activities of components A and B are constant in these regions. Hence the composition of the equilibrium vapor is constant in the two-phase regions but can vary substantially in the single-phase regions.

solid solutions have the lowest free energy and are the stable phases near the compositional extremes, while the compound AB is stable at the center. For stoichiometries between the dilute solutions and AB, the total free energy is lowest for mixtures, namely $\alpha + AB$ and $AB + \beta$. Following the dashed tie lines gives the lowest free energies attainable as x_B is varied. The chemical potential μ for a given component is defined as the change in free energy with respect to a change in the concentration of that component, i.e., the slope of the free energy with respect to composition. Hence μ varies within single-phase regions but is constant in two-phase regions. In this example, the slope changes sign over a small range of composition as the compound AB is encountered. The activities of components A and B are plotted in Fig. 12(c). Notice that the activities change dramatically as x_B varies through the AB phase region. Decomposition with fractional sublimation can be envisioned as starting at, for example, $x_B = 0.75$, where B has the higher partial pressure, and proceeding to the left until the AB boundary is reached. At that point, the partial pressure of B would drop and fractional sublimation would cease. These principles apply to the fullerides and plots like those of Fig. 12 can be drawn, with account taken of intermediate compounds.

As an alternative means of describing the phase purification process, we can consider the phase diagram for K_xC_{60} that would correspond to a pressure of 10^{-10} Torr. At this pressure, the sublimation points of C_{60} and K will occur at low temperature and Fig. 13 shows the appropriate modification compared to Fig. 10. The C_{60} sublimation point is located by examination of Fig. 1 when the equilibrium vapor pressure is 10^{-10} Torr at ~480 K. The equivalent temperature for elemental potassium is near 260 K.[74] Experimentally, we know that the A_4C_{60} compounds are the most stable fullerides, persisting to ~700 K, depending on the alkali metal. Accordingly, the sublimation line is drawn in Fig. 13 to have a maximum temperature for $x = 4$. Regions of solid- and vapor-phase coexistence are apparent from Fig. 13 at temperatures above the α-C_{60} and K sublimation points. At these temperatures, the overall stoichiometry of the sample will change as the vapor phase is produced and

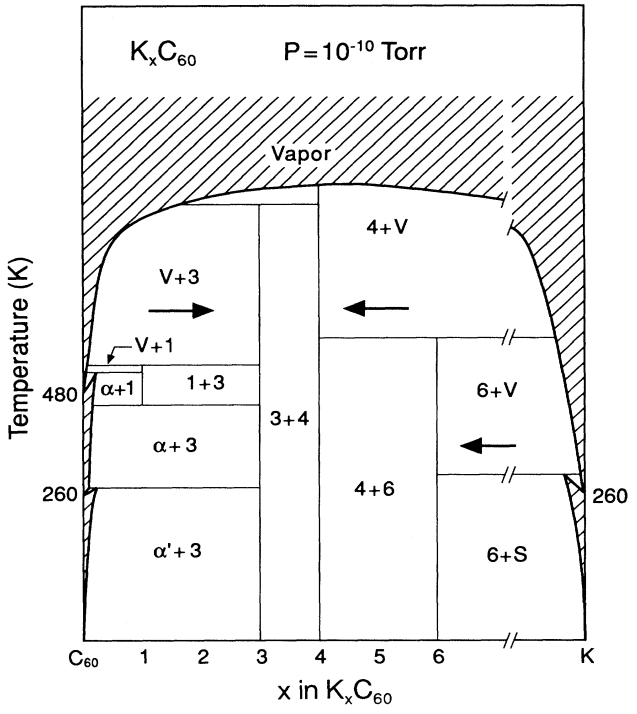

FIG. 13. Proposed phase diagram of K_xC_{60} at 10^{-10} Torr. The principal difference compared to Fig. 10 is a reduction in the temperature at which the vapor coexists with the solid for stoichiometries near the extremes of pure C_{60} and pure K. A sample with stoichiometry near $x = 1$ will evolve to K_3C_{60} when heated to ~500 K, as observed experimentally during fractional sublimation (see bold arrow at left). Likewise, heating a sample of stoichiometry $x = 6$ at ~650 K will drive off K and the final stoichiometry will be K_4C_{60}.

pumped away. For $x < 3$, the vapor is rich in C_{60} compared to the average composition, so that fractional sublimation will proceed to the right, as depicted by the large isothermal arrow. For $x > 4$, the vapor will be rich in K so that the process will carry the system to the left, again indicated with large arrows. At a given temperature, the process will stop when a single solid phase exists.

VI. CONCLUSIONS

Phase diagrams of C_{60} and the K-, Rb-, and Cs-C_{60} systems have been discussed. The binary phase diagrams exhibit considerably more complexity than originally anticipated. While we have demonstrated that the Rb_1C_{60} and Cs_1C_{60} phases have a finite range of composition, the phase boundaries of all of the fullerides remain imprecisely defined. We have proposed a plausible phase diagram, have identified system-specific differences, and have discussed the relationship of the phase diagram to decomposition reactions. It will remain for future studies to determine whether the high-temperature behavior follows our predictions.

ACKNOWLEDGMENTS

This work was supported by the National Science Foundation. D.M.P. acknowledges support by the University of Minnesota Graduate School. We are grateful for insightful discussions with J. L. Martins and D. Goetsch and for results shared prior to publication by J. E. Schirber, M. G. Mitch, M. C. Martin, Q. Zhu, and T. Kälber. Purified C_{60} was generously provided by R. E. Smalley and L. P. F. Chibante.

[1]R. C. Haddon *et al.*, Nature **350**, 320 (1991).
[2]A. F. Hebard *et al.*, Nature **350**, 600 (1991).
[3]M. J. Rosseinsky *et al.*, Phys. Rev. Lett. **66**, 2830 (1991).
[4]K. Holczer, O. Klein, S.-M. Huang, R. B. Kaner, K.-J. Fu, R. L. Whetten, and F. Diederich, Science **252**, 1154 (1991).
[5]D. M. Poirier, T. R. Ohno, G. H. Kroll, Y. Chen, P. J. Benning, J. H. Weaver, L. P. F. Chibante, and R. E. Smalley, Science **253**, 646 (1991).
[6]C. T. Chen *et al.*, Nature **352**, 603 (1991).
[7]R. Tycko, G. Dabbagh, M. J. Rosseinsky, D. W. Murphy, R. M. Fleming, A. P. Ramirez, and J. C. Tully, Science **253**, 884 (1991).
[8]T. Pichler, M. Matus, J. Kürti, and H. Kuzmany, Phys. Rev. B **45**, 13 841 (1992).
[9]W. L. Wilson, A. F. Hebard, L. R. Narasimhan, and R. C. Haddon, Phys. Rev. B **48**, 2738 (1993).
[10]J. Winter and H. Kuzmany, Solid State Commun. **53**, 1321 (1992).
[11]Q. Zhu, O. Zhou, N. Coustel, G. B. M. Vaughan, J. P. McCauley, W. J. Romanow, J. E. Fischer, and A. B. Smith III, Science **254**, 545 (1991).
[12]R. M. Fleming *et al.*, Nature **352**, 701 (1991).
[13]P. W. Stephens *et al.*, Phys. Rev. B **45**, 543 (1992).
[14]O. Zhou and D. E. Cox, J. Phys. Chem. Solids **53**, 1373 (1992).
[15]P. W. Stephens, L. Mihaly, P. L. Lee, R. L. Whetten, S.-M. Huang, R. Kaner, F. Diederich, and K. Holczer, Nature **351**, 632 (1991).
[16]P. A. Heiney, J. E. Fischer, A. R. McGhie, W. J. Romanow, A. M. Denenstein, J. P. McCauley, Jr., A. B. Smith III, and D. E. Cox, Phys. Rev. Lett. **66**, 2911 (1991).
[17]D. M. Poirier and J. H. Weaver, Phys. Rev. B **47**, 10 959 (1993).
[18]Q. Zhu, O. Zhou, J. E. Fischer, A. R. McGhie, W. J. Romanow, R. M. Strongin, M. A. Cichy, and A. B. Smith III, Phys. Rev. B **47**, 13 948 (1993).
[19]M. C. Martin, D. Koller, X. Du, P. W. Stephens, and L. Mihaly, Phys. Rev. B **49**, 10 818 (1994).
[20]A. Jánossy, O. Chauvet, S. Pekker, J. R. Cooper, and L. Forró, Phys. Rev. Lett. **71**, 1091 (1993).
[21]R. Tycko, G. Dabbagh, D. W. Murphy, Q. Zhu, and J. E. Fischer, Phys. Rev. B **48**, 9097 (1993).
[22]O. Chauvet, G. Oszlányi, L. Forro, P. W. Stephens, M. Tegze, G. Faigel, and A. Jánossy, Phys. Rev. Lett. **72**, 2721 (1994).
[23]D. M. Poirier, Appl. Phys. Lett. **64**, 1356 (1994).
[24]M. Knupfer, D. M. Poirier, and J. H. Weaver, Phys. Rev. B **49**, 8464 (1994).
[25]Y. Z. Li, M. Chander, J. C. Patrin, J. H. Weaver, L. P. F. Chibante, and R. E. Smalley, Science **253**, 429 (1991).
[26]Y. B. Zhao, D. M. Poirier, and J. H. Weaver, J. Phys. Chem. Solids **54**, 1685 (1993).
[27]P. J. Benning, F. Stepniak, and J. H. Weaver, Phys. Rev. B **48**, 9086 (1993).
[28]D. M. Poirier, T. R. Ohno, G. H. Kroll, P. J. Benning, F. Stepniak, J. H. Weaver, L. P. F. Chibante, and R. E. Smalley, Phys. Rev. B **47**, 9870 (1993).
[29]F. Stepniak, P. J. Benning, D. M. Poirier, J. H. Weaver, L. P. F. Chibante, and R. E. Smalley, Phys. Rev. B **48**, 1899 (1993).
[30]J. L. Martins and N. Troullier, Phys. Rev. B **46**, 1766 (1992).
[31]J. Abrefah, D. R. Olander, M. Balooch, and W. J. Siekhaus, Appl. Phys. Lett. **60**, 1313 (1992).
[32]R. Glang, in *Handbook of Thin Film Technology*, edited by L. I. Maissel and R. Glang (McGraw-Hill, New York, 1970), Chap. 1.
[33]C. Pan, M. P. Sampson, Y. Chai, R. H. Hauge, and J. L. Margrave, J. Phys. Chem. **95**, 2946 (1991).
[34]A. F. Hebard, R. C. Haddon, R. M. Fleming, and A. R. Kortan, Appl. Phys. Lett. **59**, 2109 (1991).
[35]N. W. Ashcroft, Nature **365**, 387 (1993).
[36]A. Cheng, M. L. Klein, and C. Caccamo, Phys. Rev. Lett. **71**, 1200 (1993).
[37]M. H. J. Hagen, E. J. Meijer, G. C. A. M. Mooij, D. Frenkel, and H. N. W. Lekkerkerker, Nature **365**, 425 (1993).
[38]G. A. Samara, J. E. Schirber, B. Morosin, L. V. Hansen, D. Loy, and A. P. Sylwester, Phys. Rev. Lett. **67**, 3136 (1991).
[39]P. A. Heiney, J. Phys. Chem. Solids **53**, 1333 (1992).
[40]M. Núñez-Regueiro, P. Monceau, and J.-L. Hodeau, Phys. Rev. Lett. **69**, 466 (1992); M. Núñez-Regueiro, L. Abello, G. Lucazeau, and J.-L. Hodeau, Phys. Rev. B **46**, 9903 (1992).
[41]F. Moshary, N. H. Chen, I. F. Silvera, C. A. Brown, H. C. Dorn, M. S. deVries, and D. S. Bethune, Phys. Lett. **188**, 163 (1992).
[42]D. W. Snoke, K. Syassen, and A. Mittelbach, Phys. Rev. B **47**, 4146 (1993).
[43]M. Núñez-Regueiro, Mod. Phys. Lett. B **6**, 1153 (1992).
[44]B. L. Zhang, C. Z. Wang, C. T. Chan, and K. M. Ho, Phys. Rev. B **48**, 11 381 (1993).

[45]S. G. Kim and D. Tománek, Phys. Rev. Lett. **72**, 2418 (1994).
[46]J. H. Weaver and D. M. Poirier, in *Solid State Physics,* edited by H. Ehrenreich and F. Spaepen (Academic, New York, 1994), Vol. 48, Chap. 1. Also see other chapters in that volume.
[47]See, for example, *Physics and Chemistry of Fullerenes, Advanced Series in Fullerenes* edited by P. W. Stephens (World Scientific, Singapore, 1993), Vol. 1.
[48]A. F. Hebard, Annu. Rev. Mater. Sci. **23**, 159 (1993).
[49]O. Zhou *et al.*, Nature **351**, 462 (1991).
[50]O. Zhou, Q. Zhu, G. B. M. Vaughan, J. E. Fischer, P. A. Heiney, N. Coustel, J. McCauley, Jr., A. B. Smith III, and D. E. Cox, in *Novel Forms of Carbon,* edited by C. L. Renschler, J. J. Pouch, and D. M. Cox, MRS Symposia Proceedings No. 270 (Materials Research Society, Pittsburgh, 1992), p. 191.
[51]T. Yildirim, O. Zhou, J. E. Fischer, N. Bykovetz, R. A. Strongin, M. A. Cichy, A. B. Smith III, C. L. Lin, and R. Jelinek, Nature **360**, 568 (1992).
[52]Y. Chabre, D. Djurado, M. Armand, W. R. Romanow, N. Coustel, J. P. McCauley, Jr., J. E. Fischer, and A. B. Smith III, J. Am. Chem. Soc. **114**, 764 (1992).
[53]L. H. Van Vlack, *Elements of Materials Science and Engineering,* 4th ed. (Addison-Wesley, Reading, MA, 1980), Chap. 9.
[54]W. D. Callister, Jr., *Materials Science and Engineering: An Introduction* (Wiley, New York, 1985), Chap. 9.
[55]J. E. Schirber, R. A. Assink, G. A. Samara, B. Morosin, and D. Loy (unpublished).
[56]T. Atake, T. Tanaka, H. Kawaji, K. Kikuchi, K. Saito, S. Suzuki, Y. Achiba, and I. Ikemoto, Chem. Phys. Lett. **196**, 321 (1992).
[57]T. Yildirim, J. E. Fischer, A. B. Harris, P. W. Stephens, D. Liu, L. Brard, R. M. Strongin, and A. B. Smith III, Phys. Rev. Lett. **71**, 1383 (1993).
[58]Z. Belahmer, P. Bernier, L. Firlej, J. M. Lambert, and M. Ribet, Phys. Rev. B **47**, 15 980 (1993).
[59]R. Tycko, J. Phys. Chem. Solids **54**, 1713 (1993).
[60]J. E. Fischer and P. A. Heiney, J. Phys. Chem. Solids **54**, 1725 (1993).
[61]S. A. Safran, in *Solid State Physics,* edited by H. Ehrenreich and D. Turnbull (Academic, New York, 1987), Vol. 40.
[62]T. Kälber, G. Zimmer, and M. Mehring (private communication).
[63]R. E. Walstedt, D. W. Murphy, and M. J. Rosseinsky, Nature **362**, 611 (1993).
[64]H. Alloul (private communication).
[65]P. H. Citrin and T. D. Thomas, J. Chem. Phys. **57**, 4446 (1972).
[66]W. Zhang, H. Zheng, and K. H. Bennemann, Solid State Commun. **82**, 679 (1992).
[67]R. W. Lof, M. A. van Veenendaal, B. Koopmans, H. T. Jonkman, and G. A. Sawatzky, Phys. Rev. Lett. **68**, 3924 (1992).
[68]A. A. Quong and M. R. Pederson, in *Novel Forms of Carbon* (Ref. 50), p. 209.
[69]*Handbook of Chemistry and Physics,* 65th ed. (CRC Press, Boca Raton, 1985).
[70]Q. Zhu (private communication).
[71]J. H. Weaver, P. J. Benning, F. Stepniak, and D. M. Poirier, J. Phys. Chem. Solids **53**, 1707 (1992).
[72]M. G. Mitch, S. J. Chase, and J. S. Lannin (private communication).
[73]R. A. Swalin, *Thermodynamics of Solids* (Wiley, New York, 1972), Chap. 9.
[74]R. E. Honig, RCA Rev. **23**, 567 (1962).